catalysts

MDPI

Article

Chromium Oxide Supported on Silicalite-1 Zeolite as a Novel Efficient Catalyst for Dehydrogenation of Isobutane Assisted by CO_2

Yajun Luo [1], Changxi Miao [2,*], Yinghong Yue [1], Weimin Yang [2], Weiming Hua [1,*] and Zi Gao [1]

1 Shanghai Key Laboratory of Molecular Catalysis and Innovative Materials, Department of Chemistry, Fudan University, Shanghai 200438, China; 15110220011@fudan.edu.cn (Y.L.); yhyue@fudan.edu.cn (Y.Y.); zigao@fuan.edu.cn (Z.G.)

2 Shanghai Research Institute of Petrochemical Technology SINOPEC, Shanghai 201208, China; yangwm.sshy@sinopec.com

* Correspondence: miaocx.sshy@sinopec.com (C.M.); wmhua@fudan.edu.cn (W.H.); Tel.: +86-21-3124-9121 (W.H.)

Received: 3 November 2019; Accepted: 6 December 2019; Published: 7 December 2019

Abstract: The chromium oxide catalysts supported on silicalite-1 zeolite (Cr/S-1) with a Cr content between 0.5% and 7% were synthesized via an incipient wetness method. The catalysts were characterized by XRD, N_2 adsorption, TEM-EDX, UV-vis, DRIFTS, ^{29}Si MAS NMR, XPS, H_2-TPR, and NH_3-TPD. The optimum 3%Cr/S-1 catalyst with 3%Cr is more active and stable than SBA-15-supported one with the same Cr content, which is a consequence of a higher content of Cr^{6+} in the fresh 3%Cr/S-1 catalyst and a higher content of Cr^{6+} retained on the former catalyst during the reaction. The 3%Cr/S-1 catalyst affords an isobutane conversion of 36.5% with 71.2% isobutene selectivity. The catalytic activity is well correlated with the content of Cr^{6+} in the fresh catalysts. Carbon dioxide displays a promoting effect on the dehydrogenation reaction.

Keywords: CO_2 assisted dehydrogenation; isobutane; silicalite-1; SBA-15

1. Introduction

Isobutene is an important industrial chemical employed to produce butyl rubber, gasoline oxygenates (e.g., ethyl tert-butyl ether), and antioxidants (e.g., butylated hydroxyanisole) [1,2]. Its two main manufacture ways which rely on the source of petroleum, i.e., steam cracking of naphtha as well as fluidized catalytic cracking, cannot meet the increasing requirements. Due to the shortage of petroleum and environmental consideration, the dehydrogenation of small alkanes to alkenes assisted by CO_2 has attracted more attention recently [3–13]. Compared to the oxidative dehydrogenation of light alkanes with O_2, the beneficial employment of CO_2 as a soft oxidant comprises improving the product selectivity as well as decreasing CO_2 emissions [14,15]. Moreover, this route opens up a new way to utilize greenhouse CO_2.

The catalysts which were attempted for isobutane dehydrogenation assisted by CO_2 includes Cr_2O_3 [11,16], V_2O_5 [10,17,18], iron oxide [19], NiO [3], and V–Mg–O [20,21]. Ding et al. found that the isobutane conversion was enhanced from 29.8% to 50.3% for the dehydrogenation over active carbon-supported chromium oxide when replacing Ar with CO_2 [16]. Cr-based catalysts were found to exhibit higher activities for dehydrogenation of small alkanes and ethylbenzene with CO_2, and mesoporous silica molecular sieves (e.g., MCM-41 and SBA-15) were usually chosen as catalyst supports owing to their high mesopore volume and surface area [6,11,22–24]. Silicalite-1 is a siliceous zeolite with MFI structure. It is generally applied in the removal of volatile organic compounds [25], separation [26], acid catalyst [27,28], and catalyst support [29–31]. Silicalite-1 exhibits higher thermal and hydrothermal

stability than SBA-15. Thus, higher catalytic stability would be expected when employing silicalite-1 as catalyst support. Herein, a novel efficient catalyst system, i.e., silicalite-1 zeolite supported chromium oxide (Cr/S-1), for CO_2 assisted dehydrogenation of isobutane was developed, and compared with the chromia catalyst supported on SBA-15 (Cr/SBA). The catalytic result of Cr/S-1 was correlated with their physico-chemical properties, and the superior performance of Cr/S-1 to Cr/SBA was revealed.

2. Results and Discussion

2.1. Catalyst Characterization

The MFI structure of the Cr/S-1 catalysts is evidenced by their XRD patterns (Figure 1), i.e., diffraction peaks at 2θ = 8.0°, 8.9°, 23.1°, 23.3°, and 24.0° [12,32]. Crystalline Cr_2O_3 cannot be observed until the Cr content reaches 7%, indicating that chromium oxide is highly dispersed on silicate-1 zeolite at a Cr content ≤3%. The 3%Cr/SBA catalyst does not show Cr_2O_3 crystallites either (Figure 1a). The good preservation of the ordered hexagonal mesoporous structure of SBA-15 upon supporting chromia is demonstrated by the SAXS patterns (Figure S1). The more homogeneous distribution of chromium on 3%Cr/S-1 than 3%Cr/SBA is verified by the HAADF STEM mapping (Figure S2).

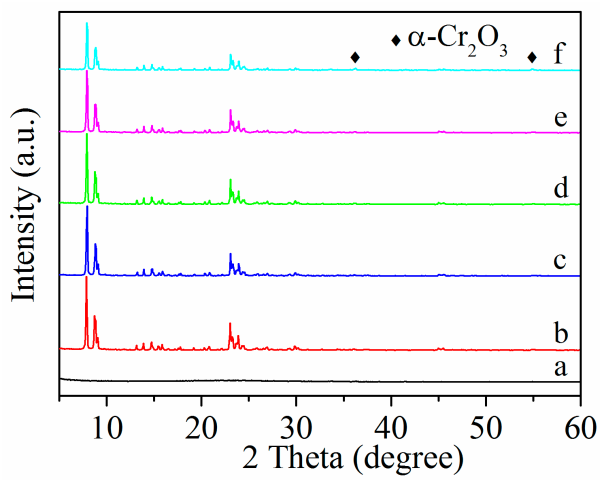

Figure 1. XRD patterns of the catalysts. (**a**) 3%Cr/SBA, (**b**) 0.5%Cr/S-1, (**c**) 1%Cr/S-1, (**d**) 2%Cr/S-1, (**e**) 3%Cr/S-1, (**f**) 7%Cr/S-1.

A surface area of 379 m^2/g observed for silicalite-1 zeolite (Table 1) is similar to the value reported in the literature [30]. As the Cr content increases from 0.5% to 3%, the surface area, microporosity and mesoporosity (contribution from silicalite-1 intercrystalline voids) of the Cr/S-1 catalysts slightly decrease (Table 1). At a high content of Cr (7%), the microporosity obviously decreases, which can be attributed to the blockage of some micropores by large chromium oxide particles (evidenced by XRD observation).

The band at 541 cm^{-1} on the Raman spectra of the Cr/S-1 and 3%Cr/SBA catalysts is characteristic of Cr_2O_3 crystallites (Figure 2) [33–35]. This band does not appear until the Cr content achieves 3% for the Cr/S-1 catalysts. The stronger intensity of this band found for the 3%Cr/SBA catalyst than 3%Cr/S-1 suggests that chromium oxide is worse dispersed on the former catalyst, which is consistent with the result of STEM mapping. The band at 983 cm^{-1} and the shoulder at 1006 cm^{-1} are related to the Cr-O stretching of monochromate and polychromate species, respectively [6,36]. The band at 603 cm^{-1} occurred in the 3%Cr/SBA catalyst is associated with a tri-siloxane ring in SBA-15 [37].

The bands at 275 and 359 nm on the diffuse reflectance UV-vis spectra of the Cr/S-1 and 3%Cr/SBA catalysts are attributed to tetrahedral Cr^{6+} species, while the ones at 458 and 599 nm are assigned to octahedral Cr^{3+} species existing in Cr_2O_3 or CrO_x clusters (Figure 3) [36,38]. The band at 599 nm cannot be found for the Cr/S-1 catalysts until the Cr content of 7%. 3%Cr/SBA shows the strongest

intensity of this band, suggesting the worse dispersion of chromium oxide on 3%Cr/SBA than 3%Cr/S-1. The above result is consistent with those of XRD and STEM mapping.

Table 1. Textural properties and H_2-TPR results of the samples.

Sample	S_{BET} (m^2/g)	V_{micro} [a] (cm^3/g)	V_{meso} (cm^3/g)	V_{total} [b] (cm^3/g)	T_M (°C)	H_2 Uptake (mmol/g)	Cr^{6+} (%) [c]
Silicalite-1	379	0.18	0.12	0.30	-	-	-
0.5%Cr/S-1	378	0.17	0.05	0.22	424	0.141	0.49
1%Cr/S-1	368	0.16	0.06	0.22	377	0.189	0.66
2%Cr/S-1	358	0.16	0.05	0.21	369	0.253	0.88
3%Cr/S-1	350	0.16	0.04	0.20	364	0.342	1.19
7%Cr/S-1	345	0.13	0.05	0.18	372 (213) [d]	0.330	1.14
SBA-15	655	0.06	1.02	1.08	-	-	-
3%Cr/SBA	469	0.02	0.69	0.71	373	0.304	1.05

[a] Calculated by the *t*-plot method; [b] Total pore volume adsorbed at P/P_0 = 0.99; [c] The weight percentage of Cr^{6+} in the sample calculated based on the H_2 consumption, assuming that Cr^{6+} was reduced to Cr^{3+} by H_2; [d] The high-temperature reduction peak and low-temperature one are 372 °C and 213 °C, respectively.

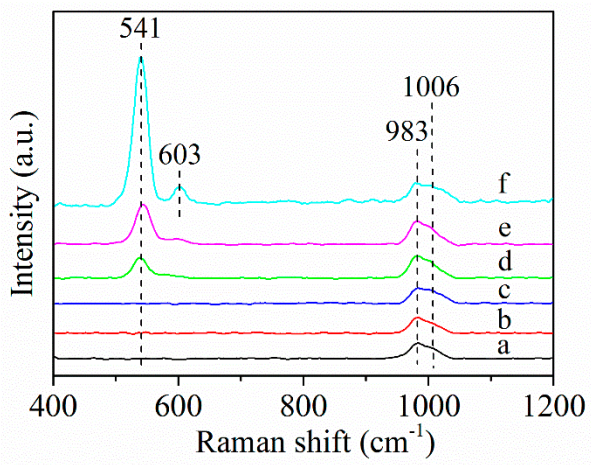

Figure 2. Raman spectra of the catalysts. (**a**) 0.5%Cr/S-1, (**b**) 1%Cr/S-1, (**c**) 2%Cr/S-1, (**d**) 3%Cr/S-1, (**e**) 7%Cr/S-1, (**f**) 3%Cr/SBA.

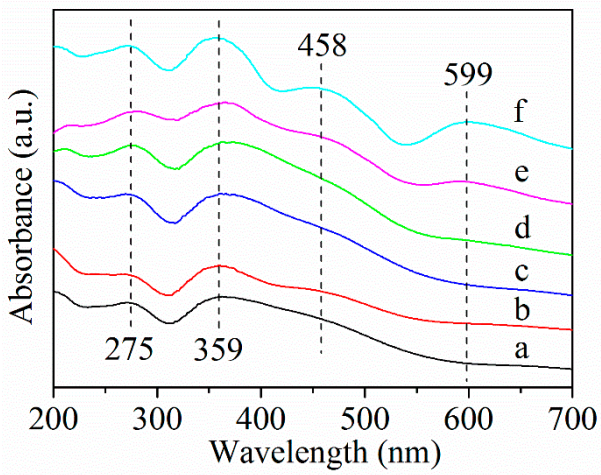

Figure 3. Diffuse reflectance UV-vis spectra of the catalysts. (**a**) 0.5%Cr/S-1, (**b**) 1%Cr/S-1, (**c**) 2%Cr/S-1, (**d**) 3%Cr/S-1, (**e**) 7%Cr/S-1, (**f**) 3%Cr/SBA.

The XPS spectra of the 3%Cr/S-1 and 3%Cr/SBA catalysts are depicted in Figure S3, and the XPS data are listed in Table 2. A remarkable decrease in the Cr^{6+} to Cr^{3+} ratio after isobutane

dehydrogenation is indicative of the reduction of most Cr^{6+} to Cr^{3+}. More Cr^{6+} was reduced to Cr^{3+} in the absence of CO_2 than in the presence of CO_2. The Cr^{6+} to Cr^{3+} ratio is greater for 3%Cr/S-1 than 3%Cr/SBA, both before and after the dehydrogenation reaction assisted by CO_2. After isobutane dehydrogenation over 3%Cr/S-1 in the absence of CO_2, followed by the treatment with CO_2 at the same temperature, the Cr^{6+} to Cr^{3+} ratio increases from 0.91 to 1.97, but it is still lower than the value of the fresh catalyst (2.82). This finding implies that CO_2 assisted isobutane dehydrogenation proceeds via a redox mechanism (Scheme 1).

Table 2. Summary of XPS data.

Sample	Sample Description	E_b (eV) [a]		Cr^{6+}/Cr^{3+} [b]
		Cr^{3+}	Cr^{6+}	
A	Fresh 3%Cr/S-1	576.9	579.2	2.82
B	Sample A reacted for 6 h in the presence of CO_2	577.1	579.5	1.19
C	Sample A reacted for 6 h in the absence of CO_2	576.7	579.6	0.91
D	Sample C subsequently treated with CO_2 at 570 °C for 0.5 h	577.0	579.4	1.97
E	Fresh 3%Cr/SBA	576.7	579.2	2.42
F	Sample E reacted for 6 h in the presence of CO_2	576.8	579.3	0.72

[a] Binding energy of Cr $2p_{3/2}$; [b] Atomic ratio of Cr^{6+} to Cr^{3+}. Reaction conditions: 570 °C, 0.1 g catalyst, CO_2 (N_2)/*i*-C_4H_{10} = 1 (mol/mol), WHSV = 4.1 h^{-1}.

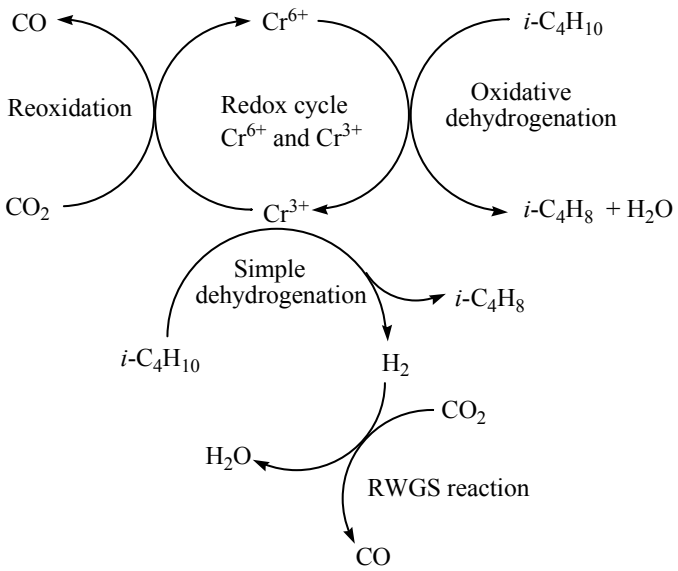

Scheme 1. Proposed reaction mechanism of isobutane dehydrogenation assisted by CO_2 over silicalite-1-supported chromium oxide catalysts.

The peak on the H_2-TPR profiles of the Cr/S-1 and 3%Cr/SBA catalysts with peak temperatures between 364 and 424 °C is assigned to the reduction of Cr^{6+} to Cr^{3+} (Figure 4) [39–41]. An additional small peak at 213 °C is observed for the 7%Cr/S-1 catalyst, indicating that large chromia crystals exist on this catalyst in addition to the dispersed chromium oxide [42]. The H_2-TPR data are presented in Table 1. The 3%Cr/S-1 catalyst exhibits a lower reduction in temperature than 3%Cr/SBA (364 °C vs. 373 °C), showing that the former catalyst displays higher reducibility than the latter one. The higher content of Cr^{6+} observed in 3%Cr/S-1 than 3%Cr/SBA (1.19% vs. 1.05%) could be related to the better dispersion of chromium species on silicalite-1 [11], as demonstrated by the STEM mapping result.

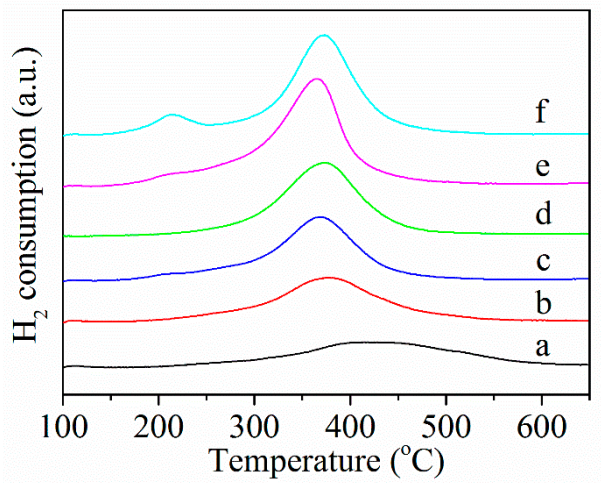

Figure 4. H_2-TPR profiles of the catalysts. (**a**) 0.5%Cr/S-1; (**b**) 1%Cr/S-1; (**c**) 2%Cr/S-1; (**d**) 3%Cr/SBA; (**e**) 3%Cr/S-1; (**f**) 7%Cr/S-1.

As revealed in Figure 5, silicalite-1 zeolite has three kinds of hydroxyl groups: Isolated silanol groups (3739 cm^{-1}), vicinal silanol groups (3686 cm^{-1}), and nest silanol groups (3493 cm^{-1}) [27,43,44]. After supporting chromium oxide, the intensities of these -OH groups, particularly the nest silanol groups, diminish. The peak area ratio of nest silanol groups to isolated silanol ones declines from 16 to 5.0 after supporting chromia (3%Cr). This observation suggests that the number of silanol groups decreases via the interaction of Cr species with the -OH groups [29,44,45]. SBA-15 has only isolated silanol groups. Supporting chromium oxide on SBA-15 also leads to a decrease in the number of hydroxyl groups. The nest silanols have a higher local density of hydroxyls than isolated silanols [46], thus resulting in a stronger interaction between chromium species and nest silanols. Therefore, the better dispersion of chromium species on silicalite-1 than SBA-15 can be attributed to the abundant nest silanol groups present on the former support.

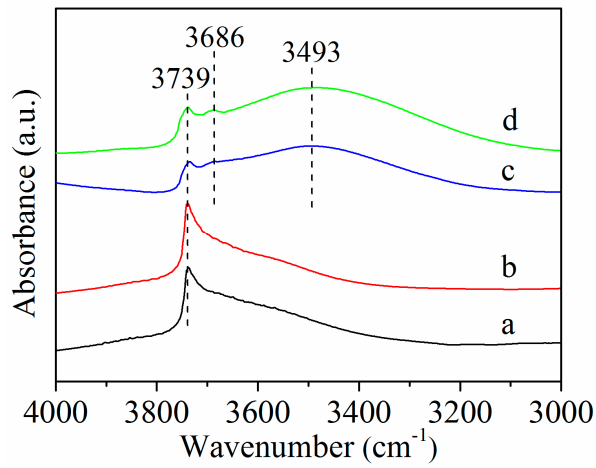

Figure 5. DRIFT spectra of some selected samples. (**a**) 3%Cr/SBA, (**b**) SBA-15, (**c**) 3%Cr/S-1, (**d**) silicalite-1.

Figure S4 presents the ^{29}Si MAS NMR spectra of some selected samples. For silicalite-1 and 3%Cr/S-1 samples, two resonances at −113 and −102 ppm correspond to Q^4 and Q^3 species representing (Si-[$(OSi)_4$]) and (HO-Si-[$(OSi)_3$]), respectively [28]. The ratio of Q^3 to Q^4 decreases from 0.108 for silicalite-1 to 0.096 for 3%Cr/S-1, indicating a loss of silanol groups. In the case of SBA-15 and 3%Cr/SBA, the broad signal can be deconvoluted into a few peaks. The peaks at ca. −90 and −100 ppm are attributed to Q^2 ($[HO]_2$-Si-[$(OSi)_2$]) and Q^3 species, respectively, while the ones below −102 ppm are

assigned to Q^4 species [23,47]. The lower (Q^2 + Q^3) to Q^4 ratio observed for 3%Cr/SBA than SBA-15 (0.272 vs. 0.341) implies a decrease in the number of hydroxyl groups.

2.2. Catalytic Performance

The catalytic results of CO_2 assisted isobutane dehydrogenation over the Cr/S-1 catalysts are shown in Figure 6 and Table 3. The effect of content of Cr in the Cr/S-1 catalysts on the initial conversion of isobutane and initial product selectivity is depicted in Figure S5. The initial isobutene selectivity declines from 79.7% to 71.2%, with increasing the Cr content from 0.5% to 3%, followed by a slight diminishment with further increasing the Cr content to 7%. The initial selectivities to C1-C3 (alkanes and alkenes) and butenes (except isobutene) follow the opposite variation trend. The activity is strongly dependent on the Cr content. The initial isobutane conversion improves markedly from 20.8% to 36.5% with increasing the Cr content from 0.5% to 3%, followed by a very slight decline in the conversion with further increasing the Cr content to 7%. The 3%Cr/S-1 catalyst displays the optimum activity, giving 36.5% isobutane conversion and 71.2% selectivity toward isobutene. As shown in Table 3, the catalyst which is more active for CO_2 assisted dehydrogenation of isobutane displays higher activity for the conversion of CO_2 to CO. The very small conversion of isobutane (ca. 3%) observed on silicalite-1 zeolite suggests that the dispersed chromium oxide on silicalite-1 is primarily responsible for the catalytic activity.

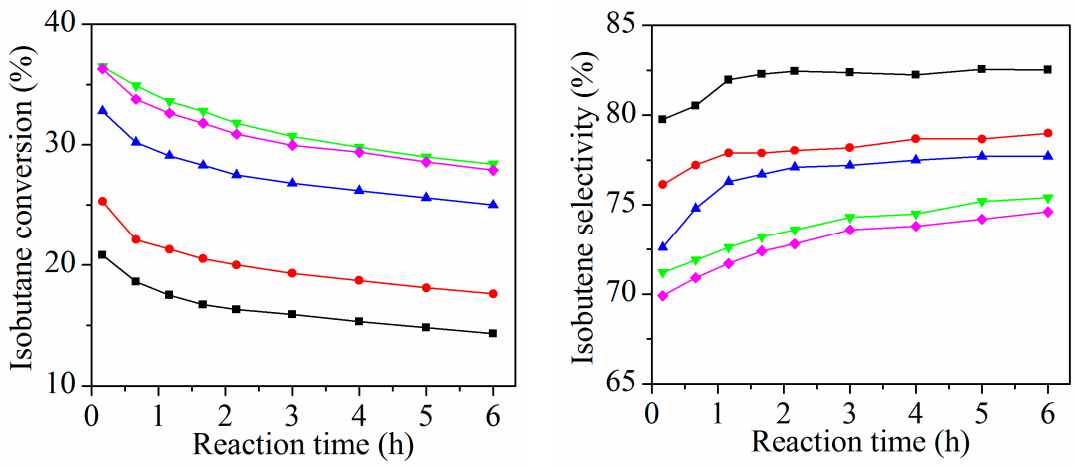

Figure 6. Catalytic performance of the Cr/S-1 catalysts for isobutane dehydrogenation assisted by CO_2 at 570 °C, (■) 0.5%Cr/S-1, (●) 1%Cr/S-1, (▲) 2%Cr/S-1, (▼) 3%Cr/S-1, (♦) 7%Cr/S-1. Reaction conditions: 570 °C, 0.1 g catalyst, CO_2/*i*-C_4H_{10} = 1 (mol/mol), WHSV = 4.1 h^{-1}.

Table 3. Reaction data of silicalite-1-supported chromium oxide catalysts [a].

Catalyst	Conversion (%)		Selectivity (%)							H_2/CO [c]
	i-C_4H_{10}	CO_2	*i*-C_4H_8	CH_4	C_2H_4	C_2H_6	C_3H_6	C_3H_8	C_4H_8 [b]	
0.5%Cr/S-1	20.8 (14.3)	3.5 (1.7)	79.7 (82.5)	3.9 (3.2)	0 (0)	0 (0)	10.7 (9.4)	0.9 (0.7)	4.8 (4.2)	4.2 (5.6)
1%Cr/S-1	25.3 (17.6)	4.8 (4.4)	76.1 (79.0)	4.8 (4.4)	0.6 (0.3)	0.4 (0.1)	10.9 (11.4)	1.3 (0.7)	5.9 (4.1)	2.6 (3.1)
2%Cr/S-1	32.8 (25.0)	10.6 (5.6)	72.6 (77.7)	5.3 (4.4)	0.7 (0.3)	0.6 (0.3)	11.0 (10.1)	1.8 (1.2)	8.0 (6.0)	1.9 (2.1)
3%Cr/S-1	36.5 (28.4)	13.3 (6.9)	71.2 (75.4)	5.6 (4.9)	0.8 (0.5)	0.9 (0.6)	11.4 (10.6)	2.0 (1.5)	8.1 (6.5)	1.8 (2.0)
7%Cr/S-1	36.3 (27.9)	11.7 (6.2)	69.9 (74.6)	5.8 (5.2)	1.0 (0.7)	1.0 (0.7)	11.6 (10.5)	2.2 (1.7)	8.5 (6.6)	2.0 (2.4)

[a] The values outside and inside the bracket are the data obtained at 10 min and 6 h, respectively; [b] Butenes excluding isobutene; [c] Molar ratio of H_2 to CO. Reaction conditions are the same as given in caption to Figure 6.

It is well accepted that CO_2 assisted dehydrogenation of small alkanes over metal oxides with redox property (e.g., chromia and vanadia) proceeds through a redox mechanism [18,22,48,49]:

$$C_nH_{2n+2} + MO_x = C_nH_{2n} + MO_{x-1} + H_2O \quad (1)$$

$$CO_2 + MO_{x-1} = CO + MO_x \quad (2)$$

The XPS results (Table 2) confirm that CO_2 assisted isobutane dehydrogenation follows the redox mechanism (Scheme 1). According to this redox mechanism, one might envisage that the Cr/S-1 catalyst having a higher amount of Cr^{6+} species would favor the dehydrogenation reaction. This hypothesis is further demonstrated by a good correlation between the initial activity and the content of Cr^{6+} in the fresh Cr/S-1 catalysts as measured by H_2-TPR (Figure 7). On the other hand, H_2 was detectable in the products. The H_2 to CO molar ratio for the Cr/S-1 catalysts is presented in Table 3. This finding suggests that besides the redox mechanism (i.e., a one-step pathway, i-C_4H_{10} + CO_2 = i-C_4H_8 + CO + H_2O), a two-step pathway also occurs during the reaction, i.e., a simple dehydrogenation of isobutane coupled with the reverse water-gas shift (RWGS) reaction (Scheme 1). The results of a separate RWGS reaction carried out at 570 °C verify that the Cr/S-1 catalysts are indeed active for this reaction (Figure S6).

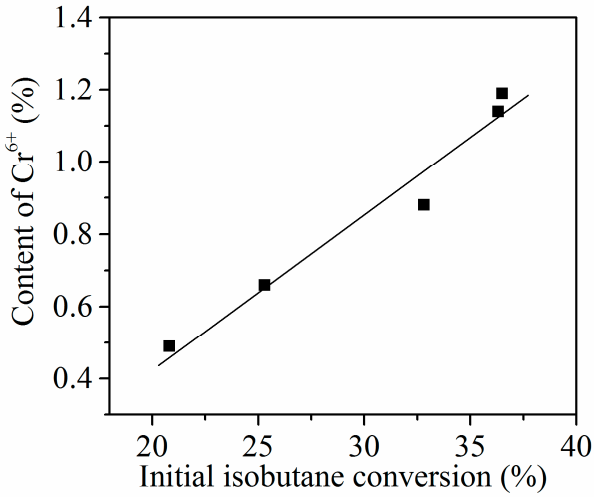

Figure 7. Correlation between the initial conversion of isobutane in the presence of CO_2 and the content of Cr^{6+} in the fresh Cr/S-1 catalysts. Reaction conditions are the same as given in caption to Figure 6.

We chose the best 3%Cr/S-1 to investigate its catalytic performance under a CO_2 or N_2 atmosphere (Figure 8). In the case of CO_2 atmosphere, this catalyst gives a 36.5% isobutane conversion with 71.2% isobutene selectivity after 10 min of reaction. In the case of N_2 atmosphere, the initial isobutane conversion and isobutene selectivity are 30.8% and 67.5%, respectively. This finding suggests that CO_2 displays a promoting effect on isobutane dehydrogenation. CO_2 enhances the dehydrogenation reaction via a redox mechanism in which the catalyst undergoes reduction (by isobutane) and reoxidation (by carbon dioxide) cycles as well as the reaction coupling between a simple dehydrogenation of isobutane and the RWGS reaction, as illustrated in Scheme 1.

A comparison of 3%Cr/S-1 and 3%Cr/SBA catalysts indicates that the initial isobutane conversion is higher on 3%Cr/S-1 than 3%Cr/SBA (Figure 9, 36.5% vs. 33.5%), which is caused by the fact that the former catalyst possesses a higher content of Cr^{6+} than the latter one (1.19% vs. 1.05%). The higher isobutene selectivity observed for 3%Cr/SBA than 3%Cr/S-1 is due to the fact that the former catalyst has lower acidity and weaker acid sites. Two desorption peaks on the NH_3-TPD profiles of both 3%Cr/S-1 and 3%Cr/SBA catalysts correspond to the weak and strong acid sites of the catalysts (Figure S7). The higher peak temperature observed for 3%Cr/S-1 than 3%Cr/SBA (393 °C vs. 320 °C) suggests that the former catalyst has stronger acid sites than the latter one. Moreover, the 3%Cr/S-1 catalyst has more acid sites than 3%Cr/SBA (0.445 vs. 0.266 mmol/g). Moreover, the 3%Cr/S-1 catalyst exhibits higher stability than 3%Cr/SBA. After 6 h of the reaction, the isobutane conversion for 3%Cr/S-1 and 3%Cr/SBA is 28.4% and 20.2%, respectively. Coking and the reduction of Cr^{6+} to Cr^{3+} are two causes responsible for the catalyst deactivation [11,50]. An in situ pretreatment of the 3%Cr/S-1 catalyst

with 10% H_2/Ar (30 mL/min) at 450 °C for 1 h leads to a decline in the initial activity from 36.5% to 32.3% (Figure 10), further confirming that the reduction of Cr^{6+} to Cr^{3+} is one of the causes for the deactivation of catalyst. The amount of coke on 3%Cr/S-1 and 3%Cr/SBA catalysts after 6 h of the reaction is 3.2% and 1.5%, respectively. The TPO profiles of both spent 3%Cr/S-1 and 3%Cr/SBA catalysts are shown in Figure S8. The peak temperature is lower for the former catalyst than the latter one (359 °C vs. 375 °C), suggesting that coke deposited on 3%Cr/S-1 is more easily burnt off. The NH_3-TPD result accounts for the higher amount of coke on 3%Cr/S-1 than 3%Cr/SBA. The XPS result shows that after the reaction, the Cr^{6+} to Cr^{3+} ratio is higher for 3%Cr/S-1 than 3%Cr/SBA (Table 2, 1.19 vs. 0.72). This result implies that the reduced chromium species which interact with the nest silanols could be more easily reoxidized to Cr^{6+} species by CO_2 during the dehydrogenation reaction. Hence, the higher catalytic stability of 3%Cr/S-1 than 3%Cr/SBA is ascribed to a higher amount of Cr^{6+} species retained during the reaction, which could be related to the abundant nest silanol groups present on the silicalite-1 support. There are no differences in the XRD patterns for the spent and fresh 3%Cr/S-1 catalysts (Figure S9), indicating the good maintenance of the catalyst structure. However, an evident diminishment in the intensity of XRD patterns for the spent 3%Cr/SBA catalyst in comparison with the fresh one was observed, suggesting a degradation of the ordered hexagonal arrangement of the SBA-15 mesopores. This is another cause for the lower catalytic stability of the 3%Cr/SBA catalyst.

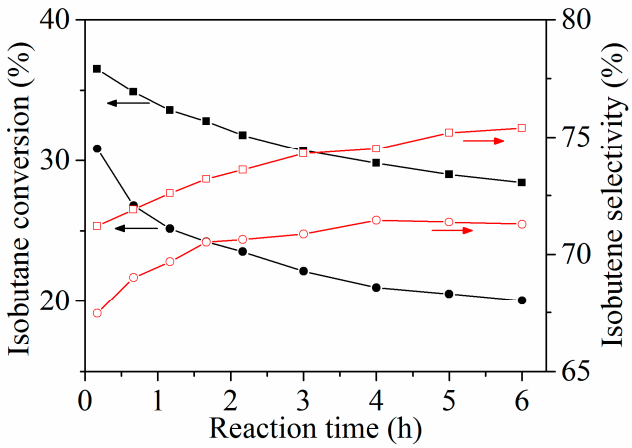

Figure 8. Conversion of isobutane and selectivity to isobutene as a function of reaction time for the 3%Cr/S-1 catalyst at 570 °C in the presence (■, □) and absence (●, ○) of CO_2. Reaction conditions: 0.1 g catalyst, CO_2 (N_2)/*i*-C_4H_{10} = 1 (mol/mol), WHSV = 4.1 h^{-1}.

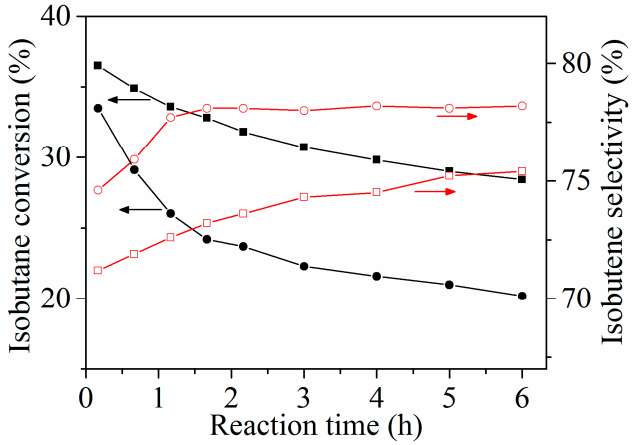

Figure 9. Conversion of isobutane and selectivity to isobutene as a function of reaction time at 570 °C in the presence of CO_2. (■, □) 3%Cr/S-1, (●, ○) 3%Cr/SBA. Reaction conditions are the same as given in caption to Figure 6.

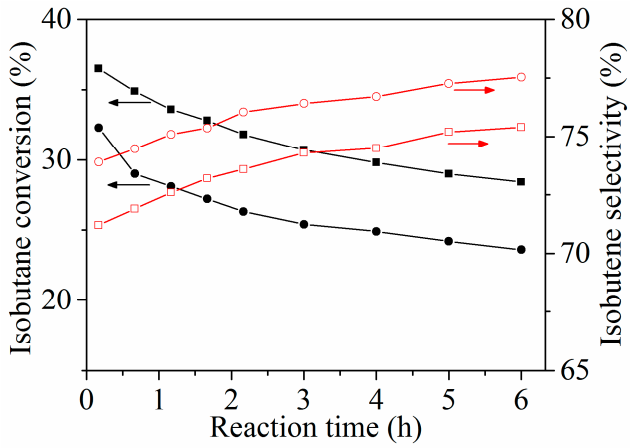

Figure 10. Conversion of isobutane and selectivity to isobutene as a function of reaction time for the 3%Cr/S-1 catalyst. (■, □) fresh catalyst, (●, ○) catalyst that was in situ pretreated by 10 vol.% H_2/Ar at 450 °C for 1 h. Reaction conditions are the same as given in caption to Figure 6.

3. Materials and Methods

3.1. Catalyst Preparation

Silicalite-1 zeolite was synthesized as follows [51]. Tetrapropylammonium hydroxide (TPAOH, 25% aqueous solution), tetraethyl orthosilicate (TEOS), and distilled water were mixed to obtain a clear suspension (9TPAOH:25SiO_2:480H_2O, molar composition). The above mixture was stirred at room temperature to hydrolyze TEOS for 4 h, followed by being transferred into an autoclave and crystallized at 170 °C for 72 h. The obtained product was filtered, washed, and dried at 100 °C overnight, followed by calcination at 550 °C for 4 h in air.

The silicalite-1-supported chromium oxide catalysts were prepared through an incipient wetness method employing $Cr(NO_3)_3{\cdot}9H_2O$ as the precursor. The impregnated samples were dried at 100 °C overnight, followed by calcination in air at 600 °C for 6 h. The obtained catalysts were designated as *x*%Cr/S-1, where *x*% represents the weight percentage of Cr in the catalysts. For the purpose of comparison, the 3%Cr/SBA catalyst (3%Cr) was prepared in the same way using SBA-15 as the support. SBA-15 was prepared according to the literature [52].

3.2. Catalyst Characterization

X-ray diffraction (XRD) measurements were performed with a D2 PHASER X-ray diffractometer (Brucker, Madison, WI, USA) at 40 mA and 40 kV. Small-angle *X*-ray scattering (SAXS) measurements were performed with a Nanostar U SAXS system (Brucker, Madison, WI, USA) using Cu Kα radiation at 35 mA and 40 kV. The surface areas and pore volumes of the catalysts were measured by N_2 adsorption on a Tristar 3000 instrument (Micromeritics, Atlanta, GA, USA). The HAADF-STEM images and elemental mapping were acquired with a Tecnai G^2 F20 S-TWIN instrument (FEI, Hillsboro, TX, USA). Diffuse reflectance ultraviolet-visible (UV-vis) spectra were collected with a Lambda 650S spectrometer (Perkin-Elmer, Waltham, MA, USA). Raman spectra were collected with an XploRA spectrometer (HORIBA Jobin Yvon, Paris, France). The exciting light wavelength was 532 nm. *X*-ray photoelectron spectroscopy (XPS) measurements were performed on a PHI 5000C spectrometer with Mg Kα radiation (Perkin-Elmer, Waltham, MA, USA). ^{29}Si MAS NMR characterization was carried out with an AVANCE III 400WB instrument (Brucker, Rheinstetten, Germany). To analyze the amount of deposited coke on the catalyst after reaction, thermogravimetric (TG) analysis was carried out in flowing air with a TGA8000 apparatus (Perkin-Elmer, Waltham, MA, USA).

Temperature-programmed desorption of NH_3 (NH_3-TPD), temperature-programmed reduction of H_2 (H_2-TPR), and temperature-programmed oxidation (TPO) characterizations were performed on an AutoChem II instrument (Micromeritics, Atlanta, GA, USA). We pretreated 0.1 g of sample (40–60 mesh)

in situ at 550 °C in N_2 flow for 1 h before the measurement. In the case of NH_3-TPD experiment, the temperature was cooled to 80 °C, and the flow was changed to 10 vol.% NH_3/He (30 mL/min) and maintained at 80 °C for 2 h, followed by being swept with He (30 mL/min) for 2 h. Then, the sample was heated in He (30 mL/min) to 600 °C at a ramp rate of 10 °C/min. In the case of H_2-TPR experiment, the temperature was cooled to 100 °C, and the flow was switched to 10% H_2/Ar (30 mL/min), followed by heating to 650 °C at a ramp rate of 10 °C/min. In the case of TPO experiment, the temperature was cooled to 150 °C, and the flow was changed to 3% O_2/He (30 mL/min), followed by heating to 650 °C at a ramp rate of 10 °C/min. Diffuse reflectance infrared Fourier transform spectroscopy (DRIFTS) spectra were recorded at 300 °C on a Nicolet 6700 spectrometer (ThermoFisher, Waltham, MA, USA) equipped with an MCT detector and a heating accessory. The sample was pretreated in situ in flowing He (30 mL/min) at 450 °C for 1 h before the measurement.

3.3. Catalytic Evaluation

Catalytic performance in CO_2 assisted dehydrogenation of isobutane was carried at 570 °C in a fixed-bed quartz tube reactor (6 mm internal diameter) under ambient pressure. The catalyst loading was 0.1 g. The catalyst (40–60 mesh) was activated in situ in N_2 flow at 570 °C for 1 h before the reaction. The feed gas contained 50 vol.% CO_2 and 50 vol.% isobutane (2.9 mL/min of isobutane), i.e., the weight hourly space velocity of 4.1 h^{-1} for isobutane. In the case of isobutane dehydrogenation in the absence of CO_2, CO_2 was replaced by N_2, while keeping the other reaction conditions the same. In the case of reverse water–gas shift reaction, the feed gas contained 50 vol.% H_2 and 50 vol.% CO_2 (2.9 mL/min of CO_2), while keeping the other reaction conditions the same. The hydrocarbon products were in-situ analyzed with a GC (FID and HP-AL/S capillary column). The column temperature was 100 °C. CO and CO_2 were in-situ analyzed with another GC (TCD and carbon molecular sieve 601 packed column). The column temperature was 70 °C. The conversion and selectivity were calculated using the standard normalization method.

4. Conclusions

In this work, we have explored the silicalite-1-supported chromium oxide catalysts for isobutane dehydrogenation assisted by CO_2. This family of catalysts is shown to be effective for the reaction. A good correlation between the initial activity of the Cr/S-1 catalysts and content of Cr^{6+} in the fresh catalysts is established. CO_2 promotes the isobutane dehydrogenation via a redox mechanism and two-step pathway. The best 3%Cr/silicalite-1 catalyst gives an isobutane conversion of 36.5% with 71.2% isobutene selectivity. The greater initial activity observed for 3%Cr/S-1 than 3%Cr/SBA is attributed to a higher content of Cr^{6+} in the fresh 3%Cr/S-1 catalyst, and the better catalytic stability for the former catalyst than the latter one is associated with a higher content of Cr^{6+} retained on the former catalyst during the reaction. This finding could be related to the abundant nest silanol groups present on the silicalite-1 support.

Supplementary Materials: The following are available online at http://www.mdpi.com/2073-4344/9/12/1040/s1, Figure S1: SAXS patterns of SBA-15 and 3%Cr/SBA, Figure S2: HAADF STEM images (left) and corresponding EDX elemental mapping of Cr (right). (a) 3%Cr/S-1; (b) 3%Cr/SBA, Figure S3: XPS spectra of Cr 2p on the fresh and spent 3%Cr/S-1 and 3%Cr/SBA catalysts. (a) fresh 3%Cr/S-1; (b) 3%Cr/S-1 after isobutane dehydrogenation in the presence of CO_2 at 570 °C for 6 h; (c) 3%Cr/S-1 after isobutane dehydrogenation in the absence of CO_2 (i.e., using N_2 instead of CO_2) at 570 °C for 6 h; (d) 3%Cr/S-1 after isobutane dehydrogenation in the absence of CO_2 at 570 °C for 6 h, followed by treatment with CO_2 at 570 °C for 0.5 h; (e) fresh 3%Cr/SBA; (f) 3%Cr/SBA after isobutane dehydrogenation in the presence of CO_2 at 570 °C for 6 h, Reaction conditions: 570 °C, 0.1 g catalyst, CO_2 (N_2)/*i*-C_4H_{10} = 1 (mol/mol), WHSV = 4.1 h^{-1}, Figure S4: ^{29}Si MAS NMR spectra of (a) Silicalite-1, (b) 3%Cr/S-1, (c) SBA-15 and (d) 3%Cr/SBA, Figure S5: The effect of content of Cr in the Cr/S-1 catalysts on the initial conversion of isobutane and initial product selectivity. Reaction conditions: 570 °C, 0.1 g catalyst, CO_2/*i*-C_4H_{10} = 1 (mol/mol), WHSV = 4.1 h^{-1}. Figure S6: The results of the reverse water gas shift reaction over the Cr/S-1 catalysts at 570 °C. (■) 0.5%Cr/S-1; (●) 1%Cr/S-1; (▲) 2%Cr/S-1; (▼) 3%Cr/S-1; (♦) 7%Cr/S-1. Reaction conditions: 0.1 g catalyst, CO_2/H_2 = 1 (mol/mol), 2.9 mL/min of CO_2. Figure S7: NH_3-TPD profiles of (a) 3%Cr/SBA and (b) 3%Cr/S-1, Figure S8: TPO profiles of both spent 3%Cr/S-1 and 3%Cr/SBA catalysts. Reaction conditions are the same as given in caption to

Figure S5. Figure S9: (a) SAXS patterns of 3%Cr/SBA and (b) XRD patterns of 3%Cr/S-1 before and after isobutane dehydrogenation assisted by CO_2. Reaction conditions are the same as given in caption to Figure S5.

Author Contributions: C.M., W.H. conceived and designed the experiments; Y.L. performed the experiments; Y.Y., W.H. and Z.G. analyzed the data; Y.L. wrote the paper; C.M., W.Y. and W.H. revised the paper.

Acknowledgments: This work was financially supported by the National Key R&D Program of China (2017YFB0602200), the National Natural Science Foundation of China (91645201), the Science and Technology Commission of Shanghai Municipality (13DZ2275200) and the Shanghai Research Institute of Petrochemical Technology SINOPEC (17ZC06070001).

Conflicts of Interest: The authors declare no conflict of interest.

References

1. Sun, J.; Zhu, K.; Gao, F.; Wang, C.; Liu, J.; Peden, C.H.F.; Wang, Y. Direct conversion of bio-ethanol to isobutene on nanosized $Zn_xZr_yO_z$ mixed oxides with balanced acid–base sites. *J. Am. Chem. Soc.* **2011**, *133*, 11096–11099. [CrossRef] [PubMed]
2. Luttrell, W.E. Isobutylene. *J. Chem. Health Saf.* **2013**, *20*, 35–37. [CrossRef]
3. Ding, J.F.; Qin, Z.F.; Li, X.K.; Wang, G.F.; Wang, J.G. Catalytic dehydrogenation of isobutane in the presence of carbon dioxide over nickel supported on active carbon. *J. Mol. Catal. A* **2010**, *315*, 221–225. [CrossRef]
4. Chen, M.; Wu, J.L.; Liu, Y.M.; Cao, Y.; Guo, L.; He, H.Y.; Fan, K.N. Study in support effect of In_2O_3/MO_x (M = Al, Si, Zr) catalysts for dehydrogenation of propane in the presence of CO_2. *Appl. Catal. A* **2011**, *407*, 20–28. [CrossRef]
5. Michorczyk, P.; Ogonowski, J.; Zenczak, K. Activity of chromium oxide deposited on different silica supports in the dehydrogenation of propane with CO_2—A comparative study. *J. Mol. Catal. A* **2011**, *349*, 1–12. [CrossRef]
6. Baek, J.; Yun, H.J.; Yun, D.; Choi, Y.; Yi, J. Preparation of highly dispersed chromium oxide catalysts supported on mesoporous silica for the oxidative dehydrogenation of propane using CO_2: Insight into the nature of catalytically active chromium sites. *ACS Catal.* **2012**, *2*, 1893–1903. [CrossRef]
7. Wu, J.L.; Chen, M.; Liu, Y.M.; Cao, Y.; He, H.Y.; Fan, K.N. Sucrose-templated mesoporous β-Ga_2O_3 as a novel efficient catalyst for dehydrogenation of propane in the presence of CO_2. *Catal. Commun.* **2013**, *30*, 61–65. [CrossRef]
8. Koirala, R.; Buechel, R.; Krumeich, F.; Pratsinis, S.E. Oxidative dehydrogenation of ethane with CO_2 over flame-made Ga-loaded TiO_2. *ACS Catal.* **2015**, *5*, 690–702. [CrossRef]
9. Rahmani, F.; Haghighi, M.; Amini, M. The beneficial utilization of natural zeolite in preparation of Cr/clinoptilolite nanocatalyst used in CO_2-oxidative dehydrogenation of ethane to ethylene. *J. Ind. Eng. Chem.* **2015**, *31*, 142–155. [CrossRef]
10. Wei, C.L.; Xue, F.Q.; Miao, C.X.; Yue, Y.H.; Yang, W.M.; Hua, W.M.; Gao, Z. Dehydrogenation of isobutane with carbon dioxide over SBA-15-supported vanadium oxide catalysts. *Catalysts* **2016**, *6*, 171. [CrossRef]
11. Wei, C.L.; Xue, F.Q.; Miao, C.X.; Yue, Y.H.; Yang, W.M.; Hua, W.M.; Gao, Z. Dehydrogenation of isobutane to isobutene with carbon dioxide over SBA-15-supported chromia-ceria catalysts. *Chin. J. Chem.* **2017**, *35*, 1619–1626. [CrossRef]
12. Cheng, Y.H.; Lei, T.Q.; Miao, C.X.; Hua, W.M.; Yue, Y.H.; Gao, Z. Ga_2O_3/NaZSM-5 for C_2H_6 dehydrogenation in the presence of CO_2: Conjugated effect of silanol. *Micropor. Mesopor. Mater.* **2018**, *268*, 235–242. [CrossRef]
13. Lei, T.Q.; Guo, H.Y.; Miao, C.X.; Hua, W.M.; Yue, Y.H.; Gao, Z. Mn-doped CeO_2 nanorod supported Au catalysts for dehydrogenation of ethane with CO_2. *Catalysts* **2019**, *9*, 119. [CrossRef]
14. Wang, S.B.; Zhu, Z.H. Catalytic conversion of alkanes to olefins by carbon dioxide oxidative dehydrogenations—A review. *Energy Fuels* **2004**, *18*, 1126–1139. [CrossRef]
15. Mukherjee, D.; Parkb, S.E.; Reddy, B.M. CO_2 as a soft oxidant for oxidative dehydrogenation reaction: An ecobenign process for industry. *J. CO2 Util.* **2016**, *16*, 301–312. [CrossRef]
16. Ding, J.F.; Qin, Z.F.; Li, X.K.; Wang, G.F.; Wang, J.G. Coupling dehydrogenation of isobutane in the presence of carbon dioxide over chromium oxide supported on active carbon. *Chin. Chem. Lett.* **2008**, *19*, 1059–1062. [CrossRef]
17. Ogonowski, J.; Skrzyńska, E. Dehydrogenation of isobutane in the presence of carbon dioxide over supported vanadium oxide catalysts. *React. Kinet. Catal. Lett.* **2006**, *88*, 293–300. [CrossRef]

18. Yuan, R.X.; Li, Y.; Yan, H.B.; Wang, H.; Song, J.; Zhang, Z.S.; Fan, W.B.; Chen, J.G.; Liu, Z.W.; Liu, Z.T.; et al. Insights into the vanadia catalyzed oxidative dehydrogenation of isobutane with CO_2. *Chin. J. Catal.* **2014**, *35*, 1329–1336. [CrossRef]
19. Shimada, H.; Akazawa, T.; Ikenaga, N.; Suzuki, T. Dehydrogenation of isobutane to isobutene with iron-loaded activated carbon catalyst. *Appl. Catal. A* **1998**, *168*, 243–250. [CrossRef]
20. Ogonowski, J.; Skrzyńska, E. Catalytic dehydrogenation of isobutane in the presence of carbon dioxide. *React. Kinet. Catal. Lett.* **2005**, *86*, 195–201. [CrossRef]
21. Ogonowski, J.; Skrzyńska, E. Activity of vanadium magnesium oxide supported catalysts in the dehydrogenation of isobutane. *Catal. Lett.* **2006**, *111*, 79–85. [CrossRef]
22. Shi, X.J.; Ji, S.F.; Wang, K. Oxidative Dehydrogenation of ethane to ethylene with carbon dioxide over Cr–Ce/SBA-15 catalysts. *Catal. Lett.* **2008**, *125*, 331–339. [CrossRef]
23. Cheng, Y.H.; Zhou, L.B.; Xu, J.X.; Miao, C.X.; Hua, W.M.; Yue, Y.H.; Gao, Z. Chromium-based catalysts for ethane dehydrogenation: Effect of SBA-15 support. *Micropor. Mesopor. Mater.* **2016**, *234*, 370–376. [CrossRef]
24. Ohishi, Y.; Kawabata, T.; Shishido, T.; Takaki, K.; Zhang, Q.H.; Wang, Y.; Takehira, K. Dehydrogenation of ethylbenzene with CO_2 over Cr-MCM-41 catalyst. *J. Mol. Catal. A* **2005**, *230*, 49–58. [CrossRef]
25. Li, J.X.; Shi, C.H.; Zhang, H.F.; Zhang, X.F.; Wei, Y.Y.; Jiang, K.; Zhang, B.G. Silicalite-1 zeolite membrane: Synthesis by seed method and application in organics removal. *Chemosphere* **2019**, *218*, 984–991. [CrossRef] [PubMed]
26. Wu, A.; Tang, C.Y.; Zhong, S.L.; Wang, B.; Zhou, J.J.; Zhou, R.F. Synthesis optimization of (h0h)-oriented silicalite-1 membranes for butane isomer separation. *Sep. Purif. Technol.* **2019**, *214*, 51–60. [CrossRef]
27. Heitmann, G.P.; Dahlhoff, G.; Hölderich, W.F. Catalytically active sites for the Beckmann rearrangement of cyclohexanone oxime to ε-Caprolactam. *J. Catal.* **1999**, *186*, 12–19. [CrossRef]
28. Lanzafame, P.; Barbera, K.; Perathoner, S.; Centi, G.; Aloise, A.; Migliori, M.; Macario, A.; Nagy, J.B.; Giordano, G. The role of acid sites induced by defects in the etherification of HMF on Silicalite-1 catalysts. *J. Catal.* **2015**, *330*, 558–568. [CrossRef]
29. Shi, L.H.; Liu, G.D.; Guo, H.C. Efficient Pt/Silicalite-1 catalyst for isomerization of *n*-heptane. *Catal. Commun.* **2017**, *101*, 111–115. [CrossRef]
30. Wang, D.; Wang, J.F.; Lu, C.Y.; Zou, X.L.; Cheng, H.W.; Ning, J.Y.; Lu, X.G.; Zhou, Z.F. Hydrogen production from coke oven gas by CO_2 reforming over a novel Ni-doped Silicalite-1. *Catal. Lett.* **2018**, *148*, 1424–1434. [CrossRef]
31. Niu, R.Y.; Liu, P.C.; Li, W.; Wang, S.; Li, J.P. High performance for oxidation of low-concentration methane using ultra-low Pd in silicalite-1 zeolite. *Micropor. Mesopor. Mater.* **2019**, *284*, 235–240. [CrossRef]
32. Sang, S.; Chang, F.; Liu, Z.; He, C.; He, Y.; Xu, L. Difference of ZSM-5 zeolites synthesized with various templates. *Catal. Today* **2004**, *93–95*, 729–734. [CrossRef]
33. Zaki, M.I.; Fouad, N.E.; Leyrev, J.; Knözinger, H. Physicochemical investigation of calcined chromia-coated silica and alumina catalysts—Characterization of chromium-oxygen species. *Appl. Catal.* **1986**, *21*, 359–377. [CrossRef]
34. Grzybowska, B.; Sloczynski, J.; Grabowski, R.; Wcislo, K.; Kozlowska, A.; Stoch, J.; Zielinski, J. Chromium oxide alumina catalysts in oxidative dehydrogenation of isobutane. *J. Catal.* **1998**, *178*, 687–700. [CrossRef]
35. Gao, B.; Luo, Y.J.; Miao, C.X.; Yue, Y.H.; Yang, W.M.; Hua, W.M.; Gao, Z. Oxidative dehydrogenation of 1-butene to 1,3-butadiene using CO_2 over Cr-SiO_2 catalysts prepared by sol-gel method. *Chem. Res. Chin. Univ.* **2018**, *34*, 609–615. [CrossRef]
36. Weckhuysen, B.M.; Wachs, I.E.; Schoonheydt, R.A. Surface chemistry and spectroscopy of chromium in inorganic oxides. *Chem. Rev.* **1996**, *96*, 3327–3349. [CrossRef]
37. Gao, X.; Bare, S.R.; Weckhuysen, B.; Wachs, I.E. In situ spectroscopic investigation of molecular structures of highly dispersed vanadium oxide on silica under various conditions. *J. Phys. Chem. B* **1998**, *102*, 10842–10852. [CrossRef]
38. Takehira, K.; Ohishi, Y.; Shishido, T.; Kawabata, T.; Takaki, K.; Zhang, Q.H.; Wang, Y. Behavior of active sites on Cr-MCM-41 catalysts during the dehydrogenation of propane with CO_2. *J. Catal.* **2004**, *224*, 404–416. [CrossRef]
39. Cherian, M.; Rao, M.S.; Yang, W.T.; Jehng, J.M.; Hirt, A.M.; Deo, G. Oxidative dehydrogenation of propane over Cr_2O_3/Al_2O_3 and Cr_2O_3 catalysts: Effects of loading, precursor and surface area. *Appl. Catal. A* **2002**, *233*, 21–33. [CrossRef]

40. Yim, S.D.; Nam, I.S. Characteristics of chromium oxides supported on TiO_2 and Al_2O_3 for the decomposition of perchloroethylene. *J. Catal.* **2004**, *221*, 601–611. [CrossRef]
41. Zhu, Q.J.; Takiguchi, M.; Setoyama, T.; Yokoi, T.; Kondo, J.N.; Tatsumi, T. Oxidative dehydrogenation of propane with CO_2 over Cr/H[B]MFI catalysts. *Catal. Lett.* **2011**, *141*, 670–677. [CrossRef]
42. Ye, X.N.; Hua, W.M.; Yue, Y.H.; Dai, W.L.; Miao, C.X.; Xie, Z.K.; Gao, Z. Ethylbenzene dehydrogenation to styrene in the presence of carbon dioxide over chromia-based catalysts. *New J. Chem.* **2014**, *28*, 373–378. [CrossRef]
43. Barbera, K.; Bonino, F.; Bordiga, S.; Janssens, T.V.W.; Beato, P. Structure-deactivation relationship for ZSM-5 catalysts governed by framework defects. *J. Catal.* **2011**, *280*, 196–205. [CrossRef]
44. Liu, G.D.; Liu, J.X.; He, N.; Miao, C.L.; Wang, J.L.; Xin, Q.; Guo, H.C. Silicalite-1 zeolite acidification by zinc modification and its catalytic properties for isobutane conversion. *RSC Adv.* **2018**, *8*, 18663–18671. [CrossRef]
45. Zhao, H.H.; Song, H.L.; Chou, L.J.; Zhao, J.; Yang, J.; Yan, L. Insight into the structure and molybdenum species in mesoporous molybdena–alumina catalysts for isobutane dehydrogenation. *Catal. Sci. Technol.* **2017**, *7*, 3258–3267. [CrossRef]
46. Zecchina, A.; Bordiga, S.; Spoto, G.; Marchese, L.; Petrini, G.; Leofanti, G.; Padovan, M. Silicalite characterization. 1. Structure, adsorptive Capacity, and IR spectroscopy of the framework and hydroxyl modes. *J. Phys. Chem.* **1992**, *96*, 4985–4990. [CrossRef]
47. Benamor, T.; Michelin, L.; Lebeau, B.; Marichal, C. Flash induction calcination: A powerful tool for total template removal and fine tuning of the hydrophobic/hydrophilic balance in SBA-15 type silica mesoporous materials. *Micropor. Mesopor. Mater.* **2012**, *147*, 370–376. [CrossRef]
48. Nakagawa, K.; Kajita, C.; Ikenaga, N.; Nishitani-Gamo, M.; Ando, T.; Suzuki, T. Dehydrogenation of light alkanes over oxidized diamond-supported catalysts in the presence of carbon dioxide. *Catal. Today* **2003**, *84*, 149–157. [CrossRef]
49. Mimura, N.; Okamoto, M.; Yamashita, H.; Oyama, S.T.; Murata, K. Oxidative dehydrogenation of ethane over Cr/ZSM-5 catalysts using CO_2 as an oxidant. *J. Phys. Chem. B* **2006**, *110*, 21764–21770. [CrossRef]
50. Zhang, F.; Wu, R.X.; Yue, Y.H.; Yang, W.M.; Gu, S.Y.; Miao, C.X.; Hua, W.M.; Gao, Z. Chromium oxide supported on ZSM-5 as a novel efficient catalyst for dehydrogenation of propane with CO_2. *Micropor. Mesopor. Mater.* **2011**, *145*, 194–199. [CrossRef]
51. Butt, T.; Tosheva, L. Synthesis of colloidal silicalite-1 at high temperatures. *Micropor. Mesopor. Mater.* **2014**, *187*, 71–76. [CrossRef]
52. Smith, M.A.; Zoelle, A.; Yang, Y.; Rioux, R.M.; Hamilton, N.G.; Amakawa, K.; Nielsen, P.K.; Trunschke, A. Surface roughness effects in the catalytic behavior of vanadia supported on SBA-15. *J. Catal.* **2014**, *312*, 170–178. [CrossRef]